Journal of Ceramic Processing Research. Vol. 14, No. 3, pp. 391~395 (2013)

J O U R N A L O F
Ceramic Processing Research

Synthesis of Ge-doped SnO_2 nanowires and their photoluminescence propertiess

Han Gil Na, Dong Sub Kwak, Yong Jung Kwon, Hong Yeon Cho and Hyoun Woo Kim*
Division of Materials Science and Engineering, Hanyang University, Seoul 133-791, Republic of Korea

We synthesized Ge-doped SnO_2 nanowires by heating a mixture of Sn and Ge powders. The dominant growth mechanisms turned out to be a vapor-solid (VS) process. Photoluminescence (PL) study at 7 K revealed that 2.2 eV-band and 2.6 eV-bands have been significantly intensified and reduced, respectively, by introducing the Ge elements. With the assistance of XPS and Raman spectra, we suggested that the intensification of 2.2 eV-band originated from the GeO_2 phase. Since XRD spectra, low-magnification transmission electron microscopy (TEM) image and selected area electron diffraction coincidentally negated the presence of crystalline GeO_2 phase, we suggest that the GeO_2 structure is mainly amorphous.

Key words: Nanowires, SnO2, Germanium, Photoluminescence.

Introduction

Tin oxide, SnO_2, is a wide band gap semiconductor (Eg = 3.6 eV) with several physical and chemical properties of interest in the field of flat panel displays [1], solid lasers [2], high-density frequency-domain optical data storage [3], planar waveguide [4], biological multicolor imaging [5], and host matrix for introducing optical active rare earth ions [6].

As in the cases of other nanostructures [7-26], low-dimensional structures of SnO_2, such as nanorods, nanobelts, nanowires and nanoparticles, have potential applications in nanoelectronics and optoelectronics, due to their novel physical and chemical properties. In particular, SnO_2 nanowires with a high volume-to-surface ratio has been intensively studied for the current use as the building blocks of gas sensors [27, 28], band-edge engineered hybrid structures for dye-sensitized solar cells [29], anodes for lithium ion batteries [30], field emission electron sources [31], and high-mobility transistors [32].

Doping of nanostructures aimed at improving the sensor properties has been often reported. For example, doping of noble metal (Pd) increased the sensor response of the SnO_2 nanowire H_2 sensors [33]. In-doped SnO_2 nanowires exhibited the excellent ethanol sensing properties [34]. Co-doped SnO_2 nanowires became highly sensitive H_2S gas sensors [35]. A room temperature NO_2 sensors has been fabricated from Ru-doped SnO_2 nanowires [36]. An excellent enzyme biosensor was prepared based on Sb-doped SnO_2 nanowires [37].

Furthermore, doping of metal elements onto SnO_2 nanowires has enhanced the electrical, magnetic, and optical properties. Al-doped SnO_2 nanowires exhibited better field emission properties with higher emission current density and lower turn-on field than pure SnO_2 nanowires [31]. The Sb-doping had significant influence on the electrical properties of SnO_2 nanowires [32]. The Cr [38] and Cu [39] doping into SnO_2 played an important role in tuning the ferromagnetism of SnO_2 nanowires [38, 39]. Also, the Al-doped SnO_2 nanowires exhibited the large blue shift of the emission band compared with undoped nanowires [40].

In the present paper, we have heated a mixture of Sn and Ge powders, aiming at obtaining the Ge-doped SnO_2 nanowires. As SnO_2/Ge composite materials, SnO_2-Ge heterojunction photovoltaic cells [41] and heterojuction diodes [42] have previously been studied. However, there has been no report on the SnO_2/Ge composite nanowires. In addition, we investigated the structural and photoluminescence (PL) properties of the as-prepared nanowires.

Experimental

In this study, Au-coated Si substrates were used. They were fabricated using Si as the starting material onto which an Au layer with a thickness of about 3 nm was deposited by ion sputtering (Emitech, K575X). The synthesis process was carried out in a horizontal quartz tube, which was inserted into a high-temperature furnace [43]. Sn and Ge nanopowders were used as the source material, which were fully mixed with a weight ratio of 1 : 1 (approximately 2 g in total),

The ceramic boat was put into a middle region of a quartz tube. A gold (Au) (about 3 nm-thick)-coated Si plate was situated on top of the ceramic boat which containing the source materials. The Au-coated side of the Si plate faced downwards, acting as a substrate for collecting the growth products. The temperature of the

*Corresponding author:
Tel : +82-10-8428-0883
Fax: +82-2-2220-0389
E-mail: hyounwoo@hanyang.ac.kr

furnace was set to 900 °C for 10 min. During the experiment, the ambient gas was flowed at a constant total pressure of 2 torr with the percentage of O_2 and Ar partial pressure being set to 3 and 97%, respectively.

The samples were investigated by X-ray diffraction (XRD, X'pert MRD-Philips) with $CuK\alpha_1$ radiation and an incidence angle of 0.5°. Scanning electron microscopy (SEM) was carried out using a Hitachi S-4300 FE-SEM. A JEOL JEM-2100F microscope was used for the transmission electron microscopy (TEM), energy-dispersive X-ray spectroscopy (EDX), and selected area electron diffraction (SAED) analyses. PL measurements were performed using a He-Cd laser line (325 nm, 55 mW) as the excitation source at room temperature at KBSI. Micro-Raman spectra were taken at room temperature using a Renishaw Raman spectromicroscope in the open air. A He-Ne laser beam with a wavelength of 633 nm was used for Raman excitation. The X-ray photoelectron spectroscopy (XPS) analyses were performed by using a VG Scientific Escalab 250 spectrometer with a monochromated AlK_α source ($h\nu = 1486.6$ eV) and charge compensation at KBSI (Korea). The binding energy (BE) were calculated using the C 1s band as the reference (284.6 eV).

Results and Discussion

Fig. 1(a) shows the SEM image of the final products obtained by heating a mixture of Sn and Ge powders. It is evident that the products comprise thin 1D rods. Fig. 1(b) shows the XRD spectrum of the product. The diffraction peaks in the XRD spectrum can be indexed to the tetragonal structure of SnO_2 (JCPDS 41-1445).

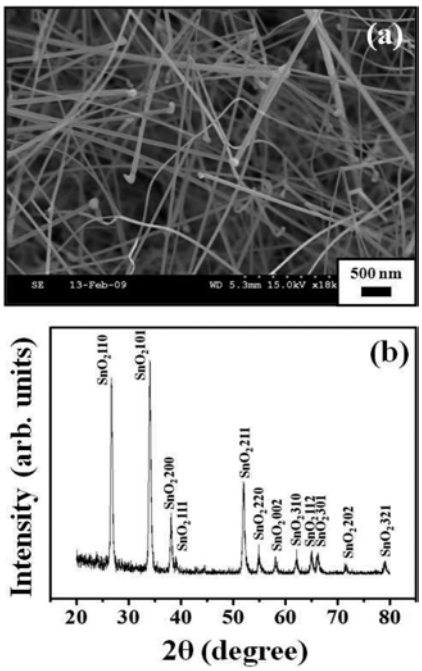

Fig. 1. (a) SEM image and (b) XRD spectrum of the product synthesized by heating a mixture of Sn and Ge powders.

The left panel of Fig. 2(a) shows a low-magnification TEM image of a nanowire, which exhibits a straight-line morphology. The right panel shows the associated SAED pattern, revealing that the nanowire has a single crystalline structure. Fig. 2(b) shows a lattice-resolved TEM image near the surface region. The interplanar spacings are about 0.21 and 0.23 nm, which correspond to the (210) and (200) planes of tetragonal SnO_2, respectively.

In order to investigate the chemical composition of the nanowire, we have carried out the EDX analysis. The left, center, and right panels of Fig. 3 show the images of the elemental maps in regard to O, Sn, and Ge elements, respectively, taken from a typical nanowire. The elemental maps reveal that the nanowire is comprised of O, Sn, and Ge elements. XRD spectrum, lattice-resolved TEM image, and SAED pattern coincidentally indicated that the nanowires are comprised of pure SnO_2 phase. However, EDX elemental mapping analysis reveals that the nanowires have Ge elements, as well as the Sn and O elements. Accordingly, it is surmise that Ge has been doped into the SnO_2 lattice without forming the crystalline GeO_2 compounds. The other possibility is that amorphous GeO_2 or GeO_x compounds have been generated.

Fig. 4(a) shows the Raman spectrum of the nanowires

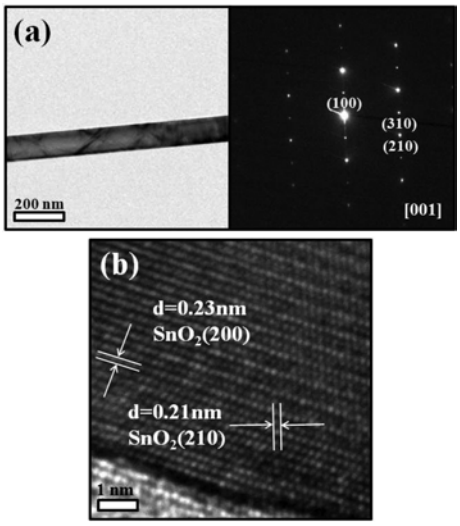

Fig. 2. (a) Low-magnification TEM image and corresponding SAED pattern of a nanowire synthesized by heating a mixture of Sn and Ge powders. (b) Lattice-resolved TEM image near the surface of the nanowire.

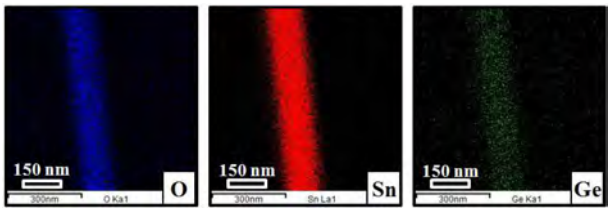

Fig. 3. TEM-EDX elemental maps of O, Sn, and Ge elements, taken from a typical nanowire.

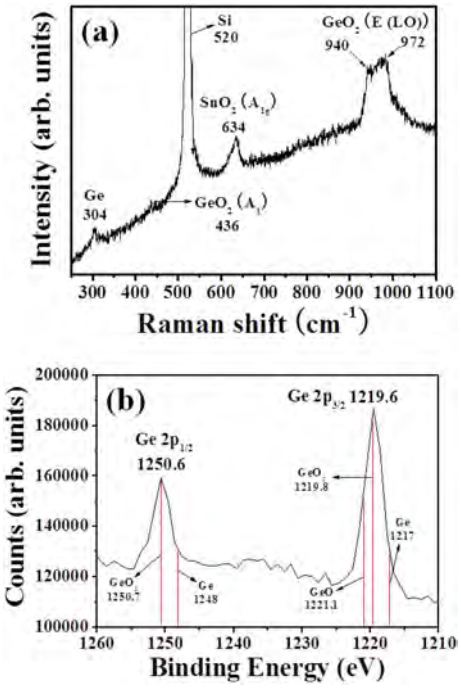

Fig. 4. (a) Room-temperature Raman spectrum of the nanowires fabricated by heating a mixture of Sn and Ge powders, in the spectral range of 250-1100 cm^{-1}. (b) XPS data for the Ge-doped SnO_2 nanowires in Ge 2p region.

produced by heating a mixture of Sn and Ge powders. The prominent peak at 520 cm^{-1} corresponds to the TO phonon mode in the silicon (Si) crystal structure [44], originated from the Si substrates. Also, the peak at 634 cm^{-1} corresponds to mode A_{1g} of SnO_2 [45]. On the other hand, the peaks at 940 cm^{-1}- and 972 cm^{-1} have been previously reported from the Raman spectra of GeO_2 [46]. In addition, there exists a peak at 436 cm^{-1}, regarded as the A_1 mode of GeO_2 [46]. The A_1 mode is due to symmetric Ge-O-Ge stretching [46]. The frequency of the Raman active optical phonons in regard to Ge is observed at 304 cm^{-1} [47]. In order to complete the above analyses, XPS was chosen to investigate the chemical binding states of Ge atoms. Fig. 4(b) shows an XPS spectrum of the Ge-doped SnO_2 nanowires, with the binding energy in the range of 1210-1260 eV. There exist two prominent peaks at 1250.6 and 1219.6 eV, respectively. Since these peaks are broad with the FWHM of about 2.40-2.75 eV, it is expected that the chemical state of Ge is present as Ge-Ge metallic bond and various oxidation states. However, among the Ge, Ge suboxides (GeO_x, $x < 2$), and GeO_2, the highest points of the peaks are closest to the lines corresponding to GeO_2. Although XPS data indicate that Ge is mainly present as GeO_2 compounds, XRD spectrum, SAED pattern, and lattice-resolved TEM image did not reveal the presence of crystalline GeO_2 phase. Accordingly, we surmise that the GeO_2 phase of the product is amorphous. The existence of amorphous GeO_2 has been previously reported [48, 49].

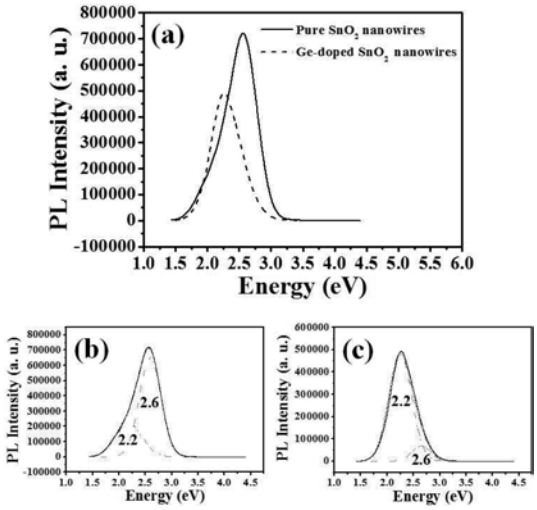

Fig. 5. (a) PL spectra of pure SnO_2 and Ge-doped SnO_2 nanowires, measured at 7 K. Gaussian-convoluted PL spectra of (b) pure SnO_2 nanowires and (c) Ge-doped SnO_2 nanowires.

Fig. 5(a) shows the PL spectra of pure SnO_2 nanowires and Ga-doped SnO_2 nanowires, respectively, measured at 7 K. Gaussian fitting analysis showed that the broad emission band of pure SnO_2 nanowires was a superimposition of two major peaks at 2.2 and 2.6 eV, respectively (Fig. 5(b)). The nature of the optical transition is generally believed to be Sn or O vacancies formed during the growth process inducing trapping states in the band gap [50]. Similarly, the best fit of the emission of Ge-doped SnO_2 nanowires was obtained with two Gaussian functions, which are centered at 2.2 and 2.6 eV, respectively (Fig. 5(c)). By comparing Fig. 5(c) with Fig. 5(b), the intensities of 2.2 eV-band and 2.6 eV-bands have been significantly increased and decreased, respectively, by introducing Ge elements. One possibility is that Ge doping into SnO_2 lattice (without forming compounds) can induce the intensification. However, there has been no previous result supporting the above mechanism. The other possibility is that the introduced Ge dopants have formed the GeO_x ($x < 2$) compounds. Previous study revealed that GeO_x mainly exhibited the PL emission around 0.8-2.2 eV [51]. Also, it is possible that the amorphous GeO_2 has been formed in the SnO_2 nanowires. Previously, the orange-green band luminescence at 2.2 eV has been observed from GeO_2 particles [52]. Accordingly, we reveal that the increase in the intensity of 2.2 eV-band is attributed to the generation of (amorphous) GeO_2 phase. On the other hand, it is not clear why the 2.6 eV-band is suppressed. We surmise that the introduced Ge elements, which generated GeO_2 compounds, will mainly reside in the outer region of the SnO_2 nanowires. Accordingly, the intensity of 2.6 eV-band from the SnO_2 will be reduced by the covering effect.

Based on the above observations, we speculated on the growth mechanism of the Ge-doped SnO_2 nanowires.

Since no Au particles are observed at the tips of the nanowires from the TEM observation, it is not possible to regard the main growth mechanism as the Au-catalyzed tip-growth vapor-solid-liquid (VLS) process. Instead, this type of growth can be ascribed to the vapor-solid (VS) mechanism. In the course of growing nanowires in the axial direction, vapors are adsorbed on the nanowire stem surface, resulting in radial growth. With the melting point of Sn (232 °C) being significantly lower than that of Ge (938 °C), the Sn-abundant nature of the vapors will result in the preferential formation of SnO_2 nanowires. In addition, SnO_2, a typical ionic compound, has a much higher melting point (MP = 1630 °C) than do Sn (MP around 232 °C), Ge (MP around 938 °C), or GeO_2 (MP around 1115 °C) [53]. Accordingly, it is reasonable to conclude that oxygen reacted first with Sn to form SnO_2. Hence, this can be another reason why SnO_2 precipitates more readily than the other three materials.

Conclusions

We fabricated a dense film of nanowires, by means of heating Sn and Ge powders. SEM and low-magnification TEM images coincidentally indicate that the nanowires have a straight-line morphology. XRD spectrum, lattice-resolved TEM image, and SAED pattern collectively reveal that the nanowires are mainly crystalline with a tetragonal rutile SnO_2 structure. In terms of TEM-EDX analyses, the elemental mapping analysis indicates that the nanowire is comprised of Ge elements, as well as Sn and O elements. Also, the Raman and XPS spectra coincidentally exhibit the characteristics of the Ge and GeO_2 structure. Since no Au particles are observed at the tips of the nanowires, this type of growth can be ascribed to the VS mechanism. The PL spectra of pure and Ge-doped SnO_2 nanowires are compared, revealing that the intensities of 2.2 eV-band and 2.6 eV-bands have been significantly increased and decreased, respectively, by introducing the Ge elements. The intensification of 2.2 eV-band by Ge incorporation is mainly ascribed to the generation of amorphous GeO_2 compound.

Acknowledgments

This research was supported by the Basic Science Research Program through the National Research Foundation (NRF) funded by the Ministry of Education, Science, and Technology (NRF-2011-0009946).

References

1. Z. Lou and J. Hao, Thin Solid Films 450 (2004) 334-340.
2. A. Biswas, G. S. Maciel, R. Kapoor, C. S. Friend and P. N. Prasad, Appl. Phys. Lett. 82 (2003) 2389-2391.
3. M. Nogami, G. Kawamura, L. Dapvril and K. Goto, Adv. Mater. 19 (2007) 2347-2350.
4. G. Ehrhart, M. Bouazaoui, B. Capoen, V. Ferreiro, R. Mahiou, O. Robbe and S. Turrell, Opt. Mater. 29 (2007) 1723-1730.
5. G.Y. Chen, Y.G. Zhang, G. Somesfalean, Z.G. Zhang, Q. Sun and F.P. Wang, Appl. Phys. Lett. 89 (2006) 163105.
6. J. Chen, J. Wang, F. Zhang, D. Yan, G. Zhang, R. Zhuo and P. Yan, J. Phys. D: Appl. Phys. 41 (2008) 105306.
7. S.-H. Lee and G.-H. Jeong, Electron. Mater. Lett. 8 (2012) 5-9.
8. J.S. Han, C. Lee and J. Lee, Electron. Mater. Lett. 8 (2012) 21-25.
9. B. Kim and B.-K. Park, Electron. Mater. Lett. 8 (2012) 33-36.
10. S.-S. Chee and J.-H. Lee, Electron. Mater. Lett. 8 (2012) 53-58.
11. S. Kim, J.-W. Jung, T.-S. Lee, S.-M. Yang and J.-R. Jeong, Electron. Mater. Lett. 8 (2012) 71-74.
12. Y. Oh, S. Nam, S. Wi, S. Hong and B. Park, Electron. Mater. Lett. 8 (2012) 91-105.
13. M. Martyniuk, G. Parish, H. Marchand, P.T. Fini, S.P. DenBaars and L. Faraone, Electron. Mater. Lett. 8 (2012) 111-115.
14. W. Czubatyj and S.J. Hudgens, Electron. Mater. Lett. 8 (2012) 157-167.
15. J. Kim, M. Eom, S. Noh and D. Shin, Electron. Mater. Lett. 8 (2012) 209-213.
16. T. Prakash, Electron. Mater. Lett. 8 (2012) 231-243.
17. Y. Chen, S.Y. Yang and J. Kim, Electron. Mater. Lett. 8 (2012) 301-304.
18. S.-S. Chee and J.-H. Lee, Electron. Mater. Lett. 8 (2012) 315-320.
19. A. Tarale, Y.D. Kolekar, V.L. Mathe, S.B. Kulkarni, V.R. Reddy and P. Joshi, Electron. Mater. Lett. 8 (2012) 381-385.
20. L. Guo, W.Y. Yoon and B.K. Kim, Electron. Mater. Lett. 8 (2012) 405-409.
21. P.L. Gong and H. Li, Electron. Mater. Lett. 8 (2012) 471-475.
22. C. Liu, Z. Liu, L. E, Y. Li, J. Han, Y. Wang, Z. Liu, J. Ya, and X. Chen, Electron. Mater. Lett. 8 (2012) 481-484.
23. S.H. Lee, H.J. Lee, H. Shiku, T. Yao and T. Matsue, Electron. Mater. Lett. 8 (2012) 511-513.
24. J. Park and K. Kim, Electron. Mater. Lett. 8 (2012) 545-548.
25. P.A. Chate, S.S. Patil, J.S. Patil, D.J. Sathe and P.P. Hankare, Electron. Mater. Lett. 8 (2012) 553-558.
26. W.-G. Lee, E. Kim and J. Jung, Electron. Mater. Lett. 8 (2012) 609-616.
27. F. Hernandez-Ramirez, J.D. Prades, A. Tarancon, S. Barth, O. Casals, R. Jimenez-Diaz, E. Pellecer, J. Rodriguez, J.R. Morante, M.A. Juli, S. Mathur and A. Romano-Rodriguez, Adv. Funct. Mater. 18 (2008) 2990-2994.
28. J.-H. Park and J.-H. Lee, Sens. Actuators B 136 (2009) 151-157.
29. S. Gubbala, V. Chakrapani, V. Lumar and M. K. Sunkara, Adv. Funct. Mater. 18 (2008) 2411-2418.
30. D.-W. Kim, I.-S. Hwang, S. J. Kwon,H.-Y. Kang, K.-S. Park, Y.-J. Choi, K.-J. Choi and J.-G. Park, Nano Lett. 7 (2007) 3041-3045.
31. L.A. Ma, Y. Ye, L.Q. Hu, K.L. Zheng and T.L. Guo, Physica E 40 (2008) 3127-3130.
32. Q. Wan, E. Dattoli and W. Lu, Small 4 (2008) 451-454.
33. Y. Shen, T. Yamazaki, Z. Liu, D. Meng, T. Kikuta, N. Nakatani, M. Saito and M. Mori, Sens. Actuators B 135(2009) 524-529.
34. X.Y. Xue, Y.J. Chen, Y.G. Liu, S.L. Shi, Y.G. Wang and T.H. Wang, Appl. Phys. Lett. 88 (2006) 201907.
35. V. Kumar, S. Sen, K.P. Muthe, N.K. Gaur, S.K. Gupta and J.V. Yakhmi, Sens. Actuators B 138 (2009) 587-590.
36. N.S. Ramgir, I.S. Mulla and K.P. Vijayamohanan, Sens.

Actuators B 107 (2005) 708-715.
37. L. Li, J. Huang, T.H. Wang, H. Zhang, Y. Liu and J.H. Li, Biosens. Bioelectron. 25 (2010) 2436-2441.
38. L. Zhang, S.H. Ge, Y. Zuo, J.A. Wang and J. Qi, Script. Mater. 63 (2010) 953-956.
39. L.J. Li, K. Yu, Z. Tang, Z.Q. Zhu and Q. Wan, J. Appl. Phys. 107 (2010) 014303.
40. M. Lei, Q.R. Hu, S.L. Wang and W.H. Tang, Mater. Lett. 64 (2010) 19-21.
41. E.Y. Wang and R.N. Legge, IEEE Trans. Electron. Dev. ED-25 (1978) 254-261.
42. R.N. Legge and E.Y. Wang, J. Appl. Phys. 51 (1980) 6035.
43. H.W. Kim, N.H. Kim, J.H. Myung and S.H. Shim, Phys. Stat. Sol. (a) 202 (2005) 1758-1762.
44. M. Hirasawa, T. Orii, and T. Seto, Appl. Phy. Lett. 88 (2006) 093119.
45. A. Dieguez, A. Romano-Rodriguez, A. Vila and J.R. Morante, J. Appl. Phys. 90 (2001) 1550-1557.
46. T.P. Mernagh and L.G. Liu, Phys. Chem. Menerals 24 (1997) 7-16.
47. M. Kumar, H.S. Mavi, S. Rath, A.K. Shukla and V.D. Vankar, Physica E 40 (2008) 2904-2910.
48. V.V. Hoang, N.H . T. Ahn and H. Zung, Phys. Stat. Sol. (b) 8 (2008) 1505-1511.
49. M. Micoulaut, L. Cormier and G.S. Henderson, J. Phys.: Condens. Matter 18 (2006) R753-R784.
50. S. Luo, J. Fan, M. Zhang, Z, Song, C. Lin, X. Wu and P.K. Chu, Nanotechnology 17 (2006) 1695-1699.
51. M. Ardyanian, H. Rinnert, X. Devaux and M. Vergnat, Appl. Phys. Lett. 89 (2006) 011902.
52. X. Zou, B. Liu, Q. Li, Z. Li, B. Li, W. Wu, Q. Zhao, Y. Sui, D. Li, B. Zou, T. Cui, G. Zou and H.-K. Mao, CrystEngComm 13 (2011) 979-984.
53. I. Barin, Thermochemical data of pure substances, 3rd ed. VCH, Weinheim, Germany (1995).